Solid-State Electronics 79 (2013) 196–200

Contents lists available at SciVerse ScienceDirect

Solid-State Electronics

journal homepage: www.elsevier.com/locate/sse

Phonon-assisted Zener tunneling in a *p–n* diode silicon nanowire

H. Carrillo-Nuñez [a,*], Wim Magnus [a,b], William G. Vandenberghe [b,c], Bart Sorée [a,b], F.M. Peeters [a]

[a] Departement Fysica, Universiteit Antwerpen, Groenenborgerlaan 171, B-2020 Antwerpen, Belgium
[b] Imec, Kapeldreef 75, B-3001 Leuven, Belgium
[c] Department of Electrical Engineering, Katholieke Universiteit Leuven, B-3001 Leuven, Belgium

ARTICLE INFO

Article history:
Received 12 April 2012
Received in revised form 5 September 2012
Accepted 7 September 2012
Available online 29 September 2012

The review of this paper was arranged by Prof. S. Cristoloveanu

Keywords:
p–n Diode
Nanowire
Phonon-assisted tunneling

ABSTRACT

The Zener tunneling current flowing through a biased, abrupt *p–n* junction embedded in a cylindrical silicon nanowire is calculated. As the band gap becomes indirect for sufficiently thick wires, Zener tunneling and its related transitions between the valence and conduction bands are mediated by short-wavelength phonons interacting with mobile electrons. Therefore, not only the high electric field governing the electrons in the space-charge region but also the transverse acoustic (TA) and transverse optical (TO) phonons have to be incorporated in the expression for the tunneling current. The latter is also affected by carrier confinement in the radial direction and therefore we have solved the Schrödinger and Poisson equations self-consistently within the effective mass approximation for both conduction and valence band electrons. We predict that the tunneling current exhibits a pronounced dependence on the wire radius, particularly in the high-bias regime.

1. Introduction

Based on the Zener tunneling or band-to-band tunneling (BTBT) mechanism, the tunnel field-effect transistor (TFET) is considered a serious candidate to conquer various performance problems encountered by the latest generations of nanometer-sized metal-oxide-semiconductor field-effect transistors (MOSFETs) [1–5]. As the electrostatic control of the latter is found to be optimal for a cylindrical wire with a channel covered by an all-round gate, its tempting to investigate the behavior of a TFET with the same geometry. As a first step, in this paper, we study BTBT tunneling in a reverse biased *p–n* diode that takes the form of a Si nanowire, a device structure which nowadays is particularly accessible by modern fabrication techniques.

In general, electronic conduction in semiconductors is negatively affected by elastic and inelastic scattering mechanisms such as electron–phonon scattering, leading to various intraband transitions that are known to degrade substantially the drive current [6–10]. On the other hand, Zener tunneling, considered as a conduction mechanism, heavily relies on interband transitions which, however, may be seriously suppressed in semiconductors with an indirect band gap, e.g. (bulk) Si. Indeed, in the latter case, the probability of a BTBT event transferring an electron from the top of the valence band (Γ-point) to the bottom of the conduction band (X-point) is negligible [11] unless the "missing" wave vector connecting Γ and X is made available. The latter can be provided by short-wavelength phonons that scatter with the transferring electrons and therefore phonon-assisted tunneling needs to be integrated into the calculation of the tunneling current. This was realized recently [12,13] for planar devices where the large electric fields were incorporated directly in the one-particle Schrödinger equation, while the electron–phonon interaction was included perturbatively up to second-order. Here, we will extend the previous formalism to cylindrical wire geometries. The proposed nanowires are not surrounded by gates and, as such, cannot be expected to exhibit any transistor action, as a real TFET would do. However, as the present paper focuses on the perspective of longitudinal BTBT as a vehicle for establishing tunneling drive currents, only z-dependent electric fields are accounted for. BTBT transitions triggered by strong, radial electric fields in gated wires, also referred to as "line tunneling" [13] will be examined elsewhere. The paper is organized as follows. In Section 2 we construct a self-consistent solution of Poisson's equation and the Schrödinger equation for electrons in both the conduction and valence band. Next, we use the resulting wave functions and energies compatible with the potential profile to modify the former expression of the tunneling current [12,13] in accordance with the cyclindrical geometry. Numerical results are presented and discussed in Section 3, and the paper is concluded in Section 4.

2. Phonon-assisted tunneling current

We consider a cylindrical *p–n* junction taking the shape of a half *p*-doped and half *n*-doped Si nanowire connected to a (reverse) bias voltage V_{pn}, as depicted in Fig. 1. The Zener tunneling current

* Corresponding author. Tel.: +32 32653545.
E-mail address: hamilton.carillonunoz@ua.ac.be (H. Carrillo-Nuñez).

0038-1101/$ - see front matter © 2012 Elsevier Ltd. All rights reserved.
http://dx.doi.org/10.1016/j.sse.2012.09.004

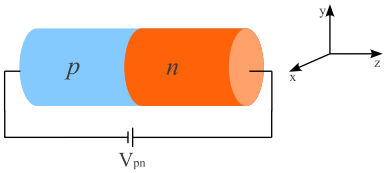

Fig. 1. *p–n* diode in a cylindrical Si nanowire.

is computed as the sum of the contributions arising from all electron transitions between different valence and conduction subbands that are due to carrier confinement in the radial direction of the nanowire. The Schrödinger equations for electrons in the different subbands for both the valence and conduction band need to be solved self-consistently together with Poisson's equation in order to determine the spatial distribution of the mobile carriers and the potential profile felt by the carriers. The latter satisfies the boundary condition from the bias voltage V_{pn}. Considering a [100]-oriented perfect cylindrical wire and adopting the effective-mass approximation, we may conveniently express the Hamiltonian for electrons in the valence (conduction) band in terms of cylindrical coordinates as

$$H_{v(c)\alpha} = \pm\frac{\hbar^2}{2m_{v(c)\alpha\perp}}\left(\frac{\partial^2}{\partial r^2}+\frac{1}{r}\frac{\partial}{\partial r}+\frac{1}{r^2}\frac{\partial^2}{\partial\phi^2}\right)\pm\frac{\hbar^2}{2m_{v(c)\alpha z}}\frac{\partial^2}{\partial z^2}+U(\mathbf{r}), \tag{1}$$

where the corresponding Schrödinger equations read

$$(E_{0v(c)}+H_{v(c)\alpha})\Psi_{v(c)\alpha}(\mathbf{r}) = E_{v(c)\alpha}\Psi_{v(c)\alpha}(\mathbf{r}), \tag{2}$$

and the valence (conduction) band edges are denoted by $E_{0v\,(c)}$, the band edge difference being equal to the band gap $E_{0c}-E_{0v}=E_g$. α is a valley index labeling various valleys within the conduction and valence bands, whereas $m_{v(c)\perp\alpha}=2m_{v(c)x\alpha}\,m_{v(c)y\alpha}/(m_{v(c)x\alpha}+m_{v(c)y\alpha})$ and $m_{v(c)z\alpha}$, respectively denote the effective mass in the planar cross section of the wire and the longitudinal effective mass in the transport direction. As detailed in Ref. [14], the effective masses $m_{v\,(c)\perp\alpha}$ and $m_{v(c)z\alpha}$ explicitly reflect the anisotropy of the conduction and valence band valleys of a [100] Si nanowire. For the sake of completeness, it should be noted that the axial symmetry of the Hamiltonian used in Eq. (2) is only approximate. Indeed, depending on the orientation of the conduction band valleys, the x and y components of the effective mass tensor, may differ and give rise to angular terms proportional to $\cos 2\phi$ and $\sin 2\phi$ when the kinetic energy operator is expressed in cylindrical coordinates. Ignoring these terms in a zeroth order approximation, one may in principle scrutinize its validity by calculating the second-order corrections to the unperturbed subband energies, as the first-order contributions vanish for symmetry reasons. On the other hand, adopting scalar effective masses for the valence band valleys, we note that both $m_{v\alpha\perp}$ and $m_{v\alpha z}$ coincide with these single, scalar masses. From the solution of the 3D Schrödinger equation, each energy eigenvalue $E_{v(c)\alpha}$ and its corresponding wave function $\Psi_{v(c)\alpha}(r,\phi,z)$ can be obtained. The potential energy $U(\mathbf{r})$ is composed of an electrostatic potential energy and an abrupt barrier at the semiconductor/oxide interface ($r=R$). As the latter is approximately taken to be infinite, it retains all carriers inside the nanowire thereby enforcing all wave functions to vanish at $r=R$. Hence, the electron concentration emerging as a weighed sum over all squared wave functions is as well bound to vanish at $r=R$. In turn, the electrostatic potential solving Poisson's equation, given the electron concentration, will in principle depend on the radial coordinate r. However, in view of the large doping levels required to produce a huge electric field in the z-direction (within the junction area), the Debye length is significantly smaller than the wire radius for radii exceeding, say 2 nm. For extremely thin wires, this argument fails, but so would the effective mass approximation. Consequently, the electron concentration is uniform in the radial direction and, hence, the radial component of the electric field is negligible except in a very narrow region near $r=R$ the contribution of which to the current density would be negligible anyway. In this light, we may safely ignore the radial dependence of the electric field and the electrostatic potential and stick to a 1D Poisson equation relating the potential energy $U(z)$ to the total charge density $\rho(z)$. As a consequence, the 3D Schrödinger equation can be reduced to a 1D equation,

$$\left(E_{0v(c)}\pm\frac{\hbar^2}{2m_{v(c)\alpha z}}\frac{\partial^2}{\partial z^2}+U(z)\right)\chi_{v(c)\alpha ml;k}(z) = (E_{v(c)\alpha}-W_{v(c)\alpha ml})\chi_{v(c)\alpha ml;k}(z). \tag{3}$$

The subband eigenfunctions and their corresponding eigenvalues $W_{v(c)\alpha ml}$ describing the subbands in the radial and azimuthal directions can be expressed as

$$\begin{aligned} R_{ml}(r,\phi) &= \frac{J_m\left(\frac{x_{ml}r}{R}\right)e^{im\phi}}{\sqrt{\pi R^2}|J_{m+1}(x_{ml})|},\\ W_{v(c)\alpha ml} &= \mp\frac{\hbar^2 x_{ml}^2}{2m_{v(c)\alpha\perp}R^2}, \end{aligned} \tag{4}$$

where x_{ml} is the lth zero of the mth Bessel function $J_m(x)$. In the transport direction, the Schrödinger equation in Eq. (3) is evaluated numerically for each subband labeled by the azimuthal and radial quantum numbers m and l, and for each longitudinal quantum number k.

The valence (conduction) band spectral function can be found from its defining expression based on the electron wave functions [12],

$$\begin{aligned} A_{v(c)}(\mathbf{r},\mathbf{r}';E) &= 2\pi\sum_{\alpha,m,l}R_{ml}(r,\phi)R_{ml}^*(r',\phi')\\ &\quad\times\sum_k\chi_{v(c)\alpha ml;k}(z)\delta(E-E_{v(c)\alpha ml;k})\chi^*_{v(c)\alpha ml;k}(z')\\ &= \sum_{\alpha,m,l}R_{ml}(r,\phi)R_{ml}^*(r',\phi')A_{v(c)\alpha ml}(z,z';E). \end{aligned} \tag{5}$$

Putting $z=z'$ in the latter, we compute the net charge density from

$$\begin{aligned} \rho(z) &= eN_D(z)-eN_A(z)+\frac{2e}{\pi R^2}\\ &\quad\times\int\frac{dE}{2\pi}\left[(1-f_v(E))\sum_{\alpha,m,l}A_{v\alpha ml}(z,z;E)-f_c(E)\sum_{\alpha,m,l}A_{c\alpha ml}(z,z;E)\right] \end{aligned} \tag{6}$$

where $N_{D(A)}$ is the donor (acceptor) doping concentration, whereas f_v and f_c respectively denote the Fermi–Dirac functions for the valence and conduction bands. Their corresponding chemical potentials are fixed by imposing charge neutrality in the source and drain regions.

Once the Schrödinger and Poisson equations are solved self-consistently, the phonon-assisted current density may be computed from [12]

$$\begin{aligned} J = -\frac{2e}{\pi R^2\hbar}\int\frac{dE}{2\pi}\Big[&(f_v(E)(1-f_c(E-\hbar\omega_{\mathbf{k}_0}))(v(\hbar\omega_{\mathbf{k}_0})+1)\\ &-f_c(E-\hbar\omega_{\mathbf{k}_0})(1-f_v(E))v(\hbar\omega_{\mathbf{k}_0}))T_v^{em}(E)\\ &+(f_v(E)(1-f_c(E+\hbar\omega_{\mathbf{k}_0}))v(\hbar\omega_{\mathbf{k}_0})\\ &-f_c(E+\hbar\omega_{\mathbf{k}_0})(1-f_v(E))(v(\hbar\omega_{\mathbf{k}_0})+1))T_v^{abs}(E)\Big] \end{aligned} \tag{7}$$

with the tunneling probability given by

$$T_{\mathrm{v}}^{\mathrm{abs,em}}(E) = \Omega|M'_{\mathbf{k}_0}|^2 \sum_{\alpha,\alpha'} \sum_{ml,m'l'} F_{ml,m'l'} \times \int \mathrm{d}z A_{\mathrm{v}\alpha'm'l'}(z,z;E) A_{\mathrm{c}\alpha ml}(z,z;E \pm \hbar\omega_{\mathbf{k}_0}) = \sum_{\alpha,\alpha'} \sum_{ml,m'l'} T^{\mathrm{abs,em}}_{\mathrm{v};\alpha ml,\alpha' m'l'}(E) \tag{8}$$

where the electron–phonon interaction is measured by $\Omega|M'_{\mathbf{k}_0}|^2$, $\Omega = \pi R^2 L_{\mathrm{W}}$ stands for the wire volume, and $\hbar\omega_{\mathbf{k}_0}$ is the phonon energy that is required for the transition between the valence band and the conduction band valley. $v(E)$ is the Bose–Einstein distribution function, while $F_{ml,m'l'}$ denotes the form factor,

$$F_{ml,m'l'} = \frac{2\pi}{\pi^2 R^4 J^2_{m+1}(x_{ml}) J^2_{m'+1}(x_{m'l'})} \int_0^R \mathrm{d}r\, r\, J^2_m\left(\frac{x_{ml} r}{R}\right) J^2_{m'}\left(\frac{x_{m'l'} r}{R}\right). \tag{9}$$

Each of the terms appearing in Eq. (7) can be straightforwardly interpreted in terms of transitions from valence to conduction band (or vice versa) assisted by the emission or absorption of a phonon [12,13]. Correspondingly, energy conservation accompanying these interband transitions and involving both intersubband scattering with wave vectors changing along the axial direction, is typically ensured by Dirac delta functions of the form $\delta(E_{\mathrm{v},l,m} - E_{\mathrm{c},l',m'} \pm \hbar\omega_{\mathbf{k}_0})$ appearing in the spectral functions, as explained in Ref. [12]. In contrast to carrier confinement being reflected in the form factors that directly affect carrier – phonon coupling, phonon confinement is ignored in this work. The justification lies in the nanowire diameter range which, throughout this paper, is deliberately chosen to exceed 4 nm. On one hand, Si nanowires in this range exhibit an indirect band gap which is a key feature for studying phonon-assisted BTBT. On the other hand, it has been found that the phonon spectra of these thicker nanowires are rapidly approaching their bulk values. For instance, Raman spectroscopy of Si nanowires [15] reveals that the width of the Gaussian confinement function which is a valuable indicator of the dependence of phonon confinement on the wire diameter, is hardly sensitive to the diameter in the range 4–25 nm.

3. Results and discussion

The Zener tunneling current is calculated for a p–n cylindrical diode Si nanowire at 300 K, as sketched in Fig. 1. The p–n junction is located at $z = 6$ nm and is considered abrupt with the p-type source and n-type drain regions being doped symmetrically up to $N_{\mathrm{A}} = N_{\mathrm{D}} = 10^{20}\ \mathrm{cm}^{-3}$, while the nanowire diameter ranges from 4 to 8 nm and its length is fixed to $L_{\mathrm{W}} = 12$ nm. In this study, the transport is assumed to be in the [100] direction. However, tunneling attributed to valleys with the heavy mass, $m_l = 0.916\ m_0$, in the transport direction [100] can be neglected. Only the contribution due to tunneling from the valence band, with (0.49, 0.49, 0.16) m_0, to the conduction band of valleys with transverse mass, $m_t = 0.19\ m_0$, in the [100] direction needs to be taken into account [11]. On the other hand, for the evaluation of the phonon-assisted tunneling probability, the transverse acoustic (TA) and transverse optical (TO) phonons provide the main contribution. For the TA branch, the electron–phonon strength is given by $\Omega|M'_{\mathbf{k}_0}|^2 = 4.86 \times 10^{-25}\ \mathrm{eV}^2\ \mathrm{cm}^3$ and the phonon energy reads $\hbar\omega_{\mathbf{k}_0} = 18.4$ meV, whereas for TO phonons we have $\Omega|M'_{\mathbf{k}_0}|^2 = 9.31 \times 10^{-25}\ \mathrm{eV}^2\ \mathrm{cm}^3$ and $\hbar\omega_{\mathbf{k}_0} = 57.6$ meV. The above parameters were taken from Ref. [11]. Fig. 2 shows a contour plot of the spectral functions for both the valence and conduction band of the cylindrical nanowire p–n diode. Not only do the spectral functions reflect the signatures of the first few subbands, they are also found to oscillate due to quantum reflections of the wave functions along the z-direction. Particularly, the electron wave function states injected respectively from the source and drain regions, are reflected by the Zener tunneling junction barrier causing interference with the injected states, while part of the wave function penetrates the barrier to decay in the opposite contact. The latter can be observed in Fig. 3 where the linear electron concentration – i.e. the number of electrons per unit length in the z direction – of the conduction and valence bands are shown for V_{pn} ranging from −0.27 V to 0.32 V. Near and inside the Zener tunneling barrier, the concentration is found to decay with a small amount of carriers residing inside the barrier region. The overlap between the corresponding states is triggering the Zener tunneling events and therefore the occurrence of the tunnel current. In Fig. 4a and b the Zener tunneling current densities are plotted separately for electrons interacting respectively with TO and TA phonons, for different nanowire radii. It turns out that the current substantially depends on the wire radius in the case of moderate backward bias ($V_{\mathrm{pn}} \approx -0.13$ V) and forward bias ($V_{\mathrm{pn}} > 0$). The current being lower in the thinner nanowires could be explained by noting that only the lowest subbands are occupied in thinner nanowires and, hence, the number of transmission channels contribution to the tunneling current is lower than in the case of thicker wires. In all cases, the presence of short-wavelength phonons is paramount to initiate interband transition whereas the direct tunneling component to the Zener current turns out to be negligible. The latter cannot be directly concluded from the present formalism which is by construction dealing only with phonon-assisted tunneling. Nevertheless, our conclusion is supported by direct comparison of the transmission coefficients $T^{\mathrm{abs}}_{\mathrm{v}}(E), T^{\mathrm{em}}_{\mathrm{v}}(E)$ with Kane's model used

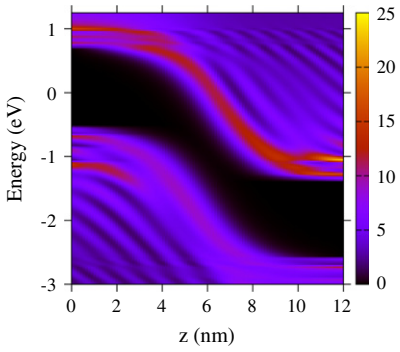

Fig. 2. Contour plot of the valence and conduction band spectral functions (expressed in $\mathrm{eV}^{-1}\ \mathrm{nm}^{-1}$) for a p–n diode in a cylindrical nanowire with length $L_{\mathrm{W}} = 12$ nm and radius $R = 2.5$ nm. The applied voltage is $V_{\mathrm{pn}} = 0.12$ V and the p–n junction is located at $z = 6$ nm.

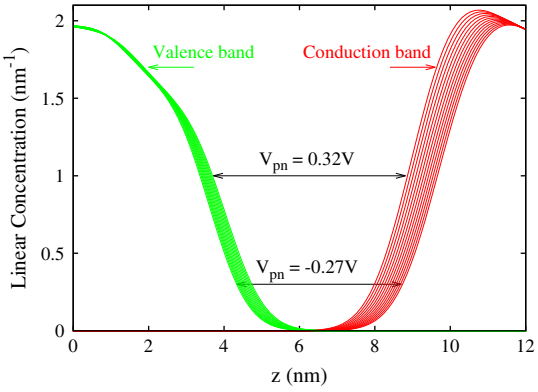

Fig. 3. Linear electron concentration for the valence (green) and conduction band (red) along the p–n junction of the cylindrical nanowire with V_{pn} ranging between −0.27 V and 0.32 V. The p–n junction is located at $z = 6$ nm. (For interpretation of the references to colour in this figure legend, the reader is referred to the web version of this article.)

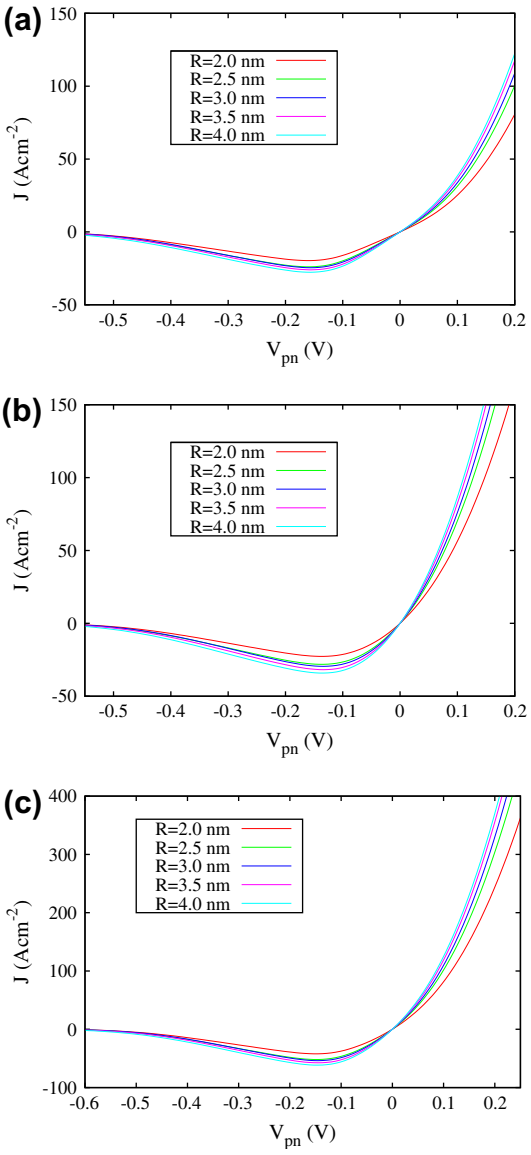

Fig. 4. Zener tunneling current density versus bias voltage calculated for different Si body radii: contribution from electrons interacting with (a) TO phonons and (b) TA phonons. The total current is shown in (c). The doping concentrations are $N_D = N_A = 10^{20}$ cm^{-3}.

for direct tunneling. Kane's transmission coefficient for a uniform electric field F at the Γ-point can be expressed as [16,17]

$$T_{\text{Kane}} = \frac{\pi^2}{9} \exp\left(-\frac{\pi E_{\text{g,direct}}^{3/2}}{4\hbar F}\sqrt{\frac{2m_0\, m_v}{m_0 + m_v}}\right) \tag{10}$$

where $E_{\text{g,direct}}$ and m_v respectively denote the direct band gap at the Γ-point and the valence band effective mass. Having adopted Si based parameter values, $m_v = 0.57m_0$, $E_{\text{g,direct}} = 3.2$ eV, we have estimated the direct transmission coefficient to be $T_{\text{Kane}} = 5 \times 10^{-11}$ where F is chosen to be the electric field at the center of the p–n junction. On the other hand, it turns out that the phonon-assisted BTBT transmission coefficient calculated in this work peaks around 5×10^{-6}, thus prominently surpassing direct tunneling by five orders of magnitude. Next, it should be noticed that, for $V_{pn} \gg 0$, the tunneling current assisted by TA phonons exceeds its counterpart due to TO phonons, especially in the high bias regime.

For the sake of comparison, we have further relaxed the infinite oxide barrier approximation and repeated the calculation for a

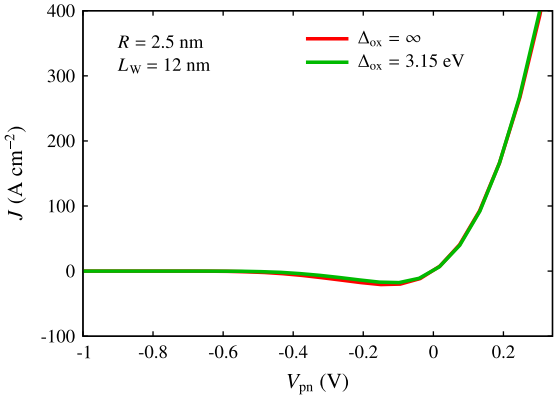

Fig. 5. Comparison of the total tunneling current calculated for a finite oxide barrier (green) and its infinite barrier counterpart (red) along the p–n junction of the cylindrical Si nanowire with $R = 2.5$ nm and $L_W = 12$ nm. Corresponding to SiO_2, the barrier height and the electron effective mass in the oxide region are resp. taken to be $\Delta = 3.15$ eV and $m_{ox} = 0.5m_0$, whereas the oxide layer thickness is assumed to be 1 nm. (For color interpretation in this figure legend the reader is referred to see the web version of this article.)

2.5 nm thick nanowire, allowing for wave function penetration into the oxide layer. The corresponding tunneling current and its infinite barrier counterpart are plotted in Fig. 5. Comparison of both curves reveals that wave function penetration and the corresponding reduction of the ground-state subband energy do not lead to substantial current enhancement, particularly in the high bias regime. Finally, one should bear in mind that all calculations presented in this work rely on the effective mass approximation. Extending the results of this paper to wire diameters significantly smaller than 4 nm, one should realize that the valley separation in the subband ladders is no longer preserved, as was demonstrated by Neophytou et. al. [18]. Hence, a more sophisticated description of the band structure, e.g. using $\mathbf{k} \cdot \mathbf{p}$ theory or tight binding techniques, would be in order.

4. Conclusion

In summary, the phonon-assisted Zener tunneling current was computed in the case of a p–n junction embedded in a cylindrical nanowire. A Schrödinger-Poisson self-consistent solution was performed in order to calculate the hole and electron spectral functions as well as the electrostatic potential. The basic expression for the tunneling current incorporates scattering between electrons and TA and TO phonons, and the calculations were repeated for different nanowire radii. As a result, the separate contributions to the current corresponding to the two phonon types as well as its dependence on the wire radius could be extracted. It is found that interband transitions caused by TA phonons provide the major contribution to the Zener tunneling current in the case of forward bias, while the contributions from TA and TO phonons are comparable in the reverse bias regime. Furthermore, penetration of the carriers into the oxide layer hardly enhances the tunneling current and does not appreciably affect the role of phonons as being the mediating mechanism. Finally, the tunneling current substantially depends on the wire radius for both moderate reverse and sufficiently large forward bias voltages.

Acknowledgments

This work is supported by the Flemish Science Foundation (FWO-VI), and the Interuniversity Attraction Poles, Belgium State, Belgium Science Policy, and IMEC. One of the authors (W. Vandenberghe) gratefully acknowledges the support of a Ph.D. stipend

from the Institute for the Promotion of Innovation through Science and Technology in Flanders (IWT-Vlaanderen).

References

[1] Banerjee S, Richardson W, Coleman J, Chatterjee A. IEEE Electron Device Lett 1987;EDL-8:347.
[2] Appenzeller J, Lin Y, Chen Z, Avouris P. IEEE Trans Electron Devices 2005;52:2568.
[3] Verhulst AS, Vandenberghe WG, Maex K, Groeseneken G. Appl Phys Lett 2007;91:053102.
[4] Luisier M, Klimeck G. IEEE Electron Device Lett 2009;30:602.
[5] Kim SH, Agarwal S, Jacobson ZA, Matheu P, Hu C, Liu TK. IEEE Electron Device Lett 2010;31:1107.
[6] Croitoru MD, Gladilin VN, Fomin VM, Devreese JT, Magnus W, Schoenmaker W, et al. J Appl Phys 1990;96:2305.
[7] Barraud S. J Appl Phys 2009;106:063714.
[8] Fischetti MV. Phys Rev B 1990;59:4901.
[9] Datta S. Electronic Transport in Mesoscopic Systems. Cambridge, UK: Cambrigde University Press; 1997.
[10] Sorée B, Magnus W, Schoenmaker W. Phys Rev B 2002;66:035318.
[11] Rivas C, Lake R, Klimeck G, Frensley WR, Fischetti MV, Thompson PE, et al. Appl Phys Lett 2001;78:814.
[12] Vanderberghe W, Sorée B, Magnus W, Fischetti MV. J Appl Phys 2011;109:124503. 12.
[13] Vanderberghe W, Sorée B, Magnus W, Groeseneken G, Fischetti MV. Appl Phys Lett 2011;98:143503. 3.
[14] Carrillo-Nuñez H, Magnus W, Peeters FM. J Appl Phys 2010;108:063708. 8.
[15] Adu KW, Guttiérrez HR, Kim UJ, Sumanasekera GU, Eklund PC. Nano Lett 2005;5:409–14.
[16] Kane EO. J Phys Chem Solids 1959;12:181–8.
[17] Kane EO. J Appl Phys 1961;32:83–91.
[18] Neophytou N, Abhijeet P, Lundstrom M, Klimeck G. IEEE Trans Electron Devices 2008;55:1286.